1

Disparate Seasonal Nitrate Export from Nested Heterogeneous Subcatchments Revealed with StorAge Selection Functions

Tam V. Nguyen[1], Rohini Kumar[2], Andreas Musolff[1], Stefanie R. Lutz[1], Fanny Sarrazin[2], Sabine Attinger[2,3], and Jan H. Fleckenstein[1,4]

[1]Department of Hydrogeology, Helmholtz Centre for Environmental Research - UFZ, 04318 Leipzig, Germany.

[2]Department of Computational Hydrosystems, Helmholtz Centre for Environmental Research - UFZ, 04318 Leipzig, Germany.

[3]Institute of Earth and Environmental Sciences, University of Potsdam, 14476 Potsdam, Germany

[4]Hydrologic Modelling Unit, Bayreuth Center of Ecology and Environmental Research (BayCEER), University of Bayreuth, 95440 Bayreuth, Germany

Corresponding author: Tam V. Nguyen (tam.nguyen@ufz.de)

Key Points:

- We introduce a novel spatially varying SAS-based model to explore nitrate export from nested subcatchments with heterogeneous settings

- Age selection preference for discharge, transit times of discharge, and nitrate export dynamics varied spatially among subcatchments

- Contrasting SAS functions between subcatchments seasonally shift the dominant source contributions to overall catchment nitrate export

24 **Abstract**

25   Understanding catchment controls on catchment solute export is a prerequisite for water
26 quality management. StorAge Selection (SAS) functions encapsulate essential information about
27 catchment functioning in terms of discharge selection preference and solute export dynamics.
28 However, they lack information on the spatial origin of solutes when applied at the catchment
29 scale, thereby limiting our understanding of the internal (subcatchment) functioning. Here, we
30 parameterized SAS functions in a spatially explicit way to understand the internal catchment
31 responses and transport dynamics of reactive dissolved nitrate (N-NO$_3$). The model was applied
32 in a nested mesoscale catchment (457 km²), consisting of a mountainous partly forested, partly
33 agricultural subcatchment, a middle-reach forested subcatchment, and a lowland agricultural
34 subcatchment. The model captured flow and nitrate concentration dynamics not only at the
35 catchment outlet but also at internal gauging stations. Results reveal disparate subsurface mixing
36 dynamics and nitrate export among headwater and lowland subcatchments. The headwater
37 subcatchment has high seasonal variation in subsurface mixing schemes and younger water in
38 discharge, while the lowland subcatchment has less pronounced seasonality in subsurface mixing
39 and much older water in discharge. Consequently, nitrate concentration in discharge from the
40 headwater subcatchment shows strong seasonality, whereas that from the lowland subcatchment
41 is stable in time. The temporally varying responses of headwater and lowland subcatchments
42 alternates the dominant contribution to nitrate export in high and low-flow periods between
43 subcatchments. Overall, our results demonstrate that the spatially explicit SAS modeling
44 provides useful information about internal catchment functioning, helping to develop or evaluate
45 spatial management practices.

1 Introduction

Agricultural practices have been identified as the main cause of poor water quality in many areas worldwide. High nitrate (N-NO$_3$) concentrations are commonly found in groundwater and surface water in areas with intensive agriculture (Randall & Mulla, 2001; Thorburn et al., 2003). Groundwater and surface water with high nitrate concentrations can negatively affect human health and the ecosystem (Boeykens et al., 2017; Knobeloch et al., 2000). In Europe, despite implemented regulations on agricultural practices (e.g., Council Directive 91/676/EEC), high nitrate concentrations in groundwater and surface water in many areas have persisted for several decades (European Commission, 2018; Knoll et al., 2019). To further develop and evaluate such regulations, understanding how catchments retain and release water and solutes (e.g., nitrate) plays an important role, especially for mesoscale catchments (10^1 – 10^4 km^2, Breuer et al., 2008) since management is often implemented at this scale (European Environment Agency, 2012).

At the mesoscale, catchments characteristics (e.g., land use, management practices, soil, topography, geological settings, and climatic conditions) are often heterogeneous (Dupas et al., 2020; Ebeling et al., 2021; Wollschläger et al., 2017). These characteristics were found to be linked to archetypal catchment solute export regimes (Ebeling et al., 2021; Musolff et al., 2015, 2017). However, in highly heterogeneous catchments, the internal (subcatchment) responses could be significantly different from the integrated catchment response, such that the integrated catchment response cannot be used to infer subcatchment behavior (Ehrhardt et al., 2019; Lassaletta et al., 2009; Scanlon et al., 2010; Winter et al., 2021). Therefore, effective spatial management of nutrient export in mesoscale catchments calls for an understanding of subcatchment functioning and its spatial integration.

In recent years, the StorAge Selection (SAS) functions concept has emerged as a useful tool to improve our mechanistic understanding of catchment functioning (Botter et al., 2011; Harman, 2019; Hrachowitz et al., 2016; Nguyen et al., 2021; Rinaldo et al., 2015; J. Yang et al., 2018). SAS functions describe catchment mixing and release of water and dissolved solutes of different ages, thus regulating the transit time distributions (TTDs) and solute composition of outflows (Botter et al., 2011; Harman, 2015; van der Velde et al., 2012). It is noted that the term "catchment mixing" (hereafter also called subsurface mixing) within the SAS function concept refers to the mixing at the catchment outlet, where water and solutes from different flow paths/ages eventually exit the catchment. SAS functions are typically incorporated into catchment-scale transport models in a lumped approach and rarely used in a distributed approach. The lumped approach (catchment-scale SAS functions) represents the integrated response of the catchment (Benettin et al., 2013; Nguyen et al., 2021), tracing the temporal dynamics of dissolved solutes in discharge at the catchment outlet, but not their explicit spatial origin. It remains unclear, to what extent parameters obtained from the spatially lumped approach are transferable to the subcatchment scale given potentially different subcatchment responses, as previously mentioned.

A spatially distributed SAS approach accounts for spatial heterogeneity in mesoscale catchments and can thus provide insights into subcatchment functioning and the spatiotemporal origin of solutes in outflows. In the distributed approach, SAS functions are applied for each model grid cell. Different implementations of the distributed SAS approach have been proposed. For example, Nguyen et al. (2021) used the non-well mixed SAS functions for for each individual grid cell. Remondi et al. (2018) used several well-mixed SAS functions for different

91   vertical storage compartments within a grid cell. Although the well-mixed assumption is applied
92   for each vertical storage compartment, the overall response of the grid cell could be far from
93   well-mixed (Benettin et al., 2017; Remondi et al., 2018). These approaches could reasonably
94   represent solute export at the catchment outlet (Nguyen et al., 2021) as well as the internal
95   gauging stations (Remondi et al., 2018). The aforementioned applications of the distributed
96   approach are limited to either catchment with homogeneous geological settings (Nguyen et al.,
97   2021) or to transport of conservative solutes (Remondi et al., 2018), while applications of these
98   approaches for catchments with heterogeneous geological settings and non-conservative solutes
99   (e.g., nitrate) are still lacking. While numerical studies have been able to provide insights into the
100   functional forms of SAS functions (which represent subsurface mixing dynamics) at the
101   catchment scale (e.g., J. Yang et al., 2018), the functional forms and spatial variability of SAS
102   functions at the grid-scale largely remain unknown. Furthermore, direct verification of the
103   functional forms of SAS functions for each grid cell (e.g., using numerical groundwater models
104   with particle tracking) would be technically/computationally very demanding if at all feasible.
105   Therefore, a semi-distributed SAS approach, in which a few SAS compartments represent
106   distinct subcatchments, may represent a reasonably sized modeling unit for which we can
107   establish sufficient process understanding to verify SAS functions and solute concentrations.

108   We hypothesize that a semi-distributed SAS approach can capture the spatial
109   heterogeneity of the catchment at an intermediate level and provide an understanding of
110   subcatchment functioning. With the semi-distributed SAS approach, SAS functions at the
111   subcatchment level can be validated (1) indirectly using instream solute/tracer concentrations at
112   the internal gauging stations or (2) directly using numerical groundwater models (if necessary).
113   Despite the potential benefits of the semi-distributed approach as mentioned above or elsewhere
114   (Hrachowitz et al., 2016; Nguyen et al., 2021), an application or implementation of this concept
115   has not yet been attempted. In addition, the temporal dynamics of SAS functions in large
116   catchments have not been given enough attention with SAS-based models. Previous studies have
117   restricted the temporal changes of SAS functions between (1) young (2) old, or (3) both young
118   and old water selection preference schemes (Nguyen et al., 2021; van der Velde et al., 2015),
119   while more selection preference schemes could exist (J. Yang et al., 2018).

120   Considering the aforementioned issues, the main objective of this research is to provide a
121   mechanistic understanding of nitrate export dynamics from a nested mesoscale catchment using
122   the SAS approach. For this purpose, we modified the mHM-SAS model (Nguyen et al., 2021) to
123   enable its application in a semi-distributed manner and to improve the representation of the
124   temporal dynamics of SAS functions. The modified model is used to explore subcatchment
125   functioning in terms of nitrate export dynamics in a mesoscale catchment with three nested
126   subcatchments located in Central Europe with a total area of 457 km^2. We also evaluate if a
127   spatially lumped SAS approach could be used for understanding subcatchment functioning,
128   especially in terms of nitrate export. Through this study, we aim at advancing the application of
129   spatially explicit SAS-based models for mesoscale heterogeneous catchments, thereby informing
130   the design of management strategies that tackle nitrate-related issues at both local and regional
131   scales.

132 **2 Methodology**

133   2.1 The mHM-SAS model

134   The mHM-SAS model (Nguyen et al., 2021) consists of a spatially distributed soil
135 nitrogen model and a spatially lumped or distributed nitrate transport model for the subsurface
136 below the soil/root zone (Figure 1). The mHM-SAS model uses the hydrological model of the
137 mesoscale Hydrologic Model (mHM, Kumar et al., 2013; Samaniego et al., 2010), the soil
138 nitrogen model of the HYdrological Predictions for the Environment model (HYPE; Lindström
139 et al., 2010; X. Yang et al., 2018), and the subsurface transport model with SAS functions (van
140 der Velde et al., 2012). The mHM-SAS model allows applying SAS functions for (1) the
141 subsurface (representing the saturated and unsaturated zones below the soil/root zone) over the
142 entire catchment (lumped SAS approach) or (2) the subsurface of each model grid cell
143 (distributed SAS approach).

144   Within the soil zone, the mHM-SAS model considers the transformation of nitrogen (N)
145 between different N pools (dissolved inorganic nitrogen - DIN, dissolved organic nitrogen -
146 DON, active organic nitrogen - SON_A, and inactive organic nitrogen - SON_I) via mineralization,
147 dissolution, and degradation. DIN is assumed to be exclusively composed of nitrate ($N-NO_3$) (X.
148 Yang et al., 2018). Nitrate is transported with water from the soil zone to the subsurface (below
149 the soil zone) and eventually to the stream. In this study, we focus on the transport of nitrate in
150 the subsurface. Using a first-order reaction for subsurface denitrification, the nitrate
151 concentration in discharge is calculated as follows:

152    $$C_Q(t) = \int_0^{+\infty} C_J(t-T,T) \cdot \exp(-k \cdot T) \cdot p_Q(t,T) \cdot dT \qquad (1)$$

153 where $C_J(t-T,T)$ [ML^{-3}] is the nitrate concentration in percolating water $J(t-T)$ [L^3T^{-1}] to the
154 SAS compartment at time $(t-T)$ [T], k [T^{-1}] is the first-order denitrification rate constant,
155 $p_Q(t,T)$ [T^{-1}] is the transit time distribution (TTD) at time t, and T [T] is the age of water since
156 its entry to the SAS compartment. The TTD, $p_Q(t,T)$ [T^{-1}], is related to the residence time
157 distribution (in form of the normalized age-ranked storage, P_S [-]; (Benettin & Bertuzzo, 2018)
158 via the SAS functions $\omega_Q(P_S,t)$ [-] as follows:

159    $$p_Q(t,T) = \omega_Q(P_S,t) \cdot \frac{\partial P_S}{\partial T} \qquad (2)$$

160   2.2. The modified mHM-SAS model

161   In this study, we modified the mHM-SAS model to enable a semi-distributed SAS
162 approach. The subcatchments were used as the spatial units for which the SAS functions are
163 applied. This is in line with the common idea that SAS functions are catchment-scale descriptors
164 (Botter et al., 2011; van der Velde et al., 2012). Subcatchment delineation should not only be
165 based on the surface or subsurface drainage area but also ensure a certain uniformity in
166 topography, land use, and geological settings. Therefore, there is no unique way to define the
167 subcatchment size, which is further discussed in detail in the case study (Section 2.3).

168   In the semi-distributed SAS approach, incoming fluxes to the SAS compartment from the
169 grid cells need to be aggregated following the subcatchment delineation. Further modifications
170 were added to account for instream processes as instream nitrate removal could be significant
171 (e.g., Alexander et al., 2000) and instream nitrate dynamics are different from subsurface solute
172 dynamics. For streamflow routing, we adopted the Muskingum-Cunge method (Cunge, 1969),

173   which was implemented in the Soil and Water Assessment Tool (SWAT, Neitsch et al., 2011). In
174   this study, instream nitrate removal via denitrification and uptake are lumped into the instream
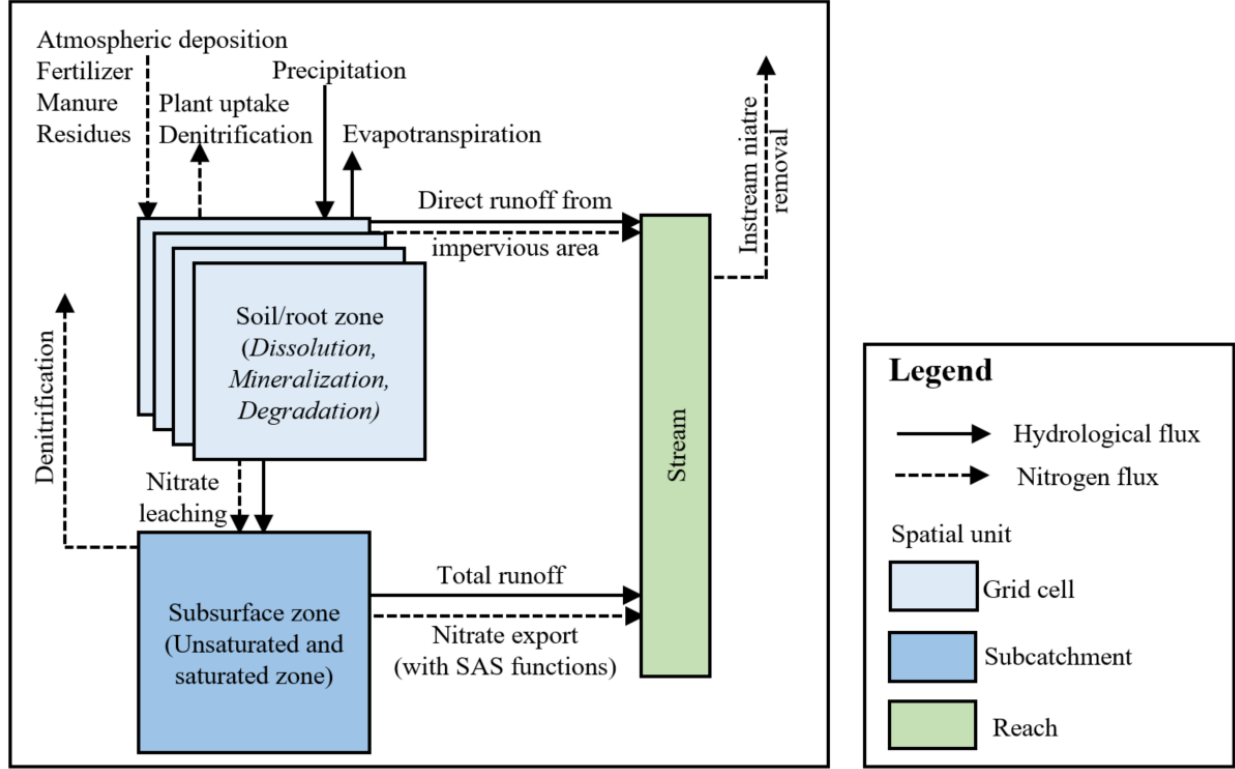175   denitrification as described by Lindström et al., (2010) and X. Yang et al. (2018).

176

178   **Figure 1**. The modified mHM-SAS model (Nguyen et al., 2021) with added instream processes.

179   Furthermore, we modified the parameterization of SAS functions in the mHM-SAS
180   model. In this study, we focus on the two-parameter beta function (Equation 3) because of its
181   flexibility in representing different types of selection preferences for outflows and its practical
182   use (Buzacott et al., 2020; Nguyen et al., 2021; van der Velde et al., 2015; J. Yang et al., 2018).
183   In previous studies, the temporal variability of the beta function parameters was restricted to
184   certain limited types of selection preferences. For example, van der Velde et al., (2012) fixed one
185   parameter of the beta function as a constant, limiting the selection preference to either (1) young
186   or (2) old water preferences according to catchment storage. Nguyen et al. (2021) used a step
187   function to represent the temporal changes of the selection preference scheme (the beta function)
188   for young or old (or both young and old) water in storage based on changes in the antecedent
189   hydrologic conditions (the ratio between the accumulated inflow and outflow over previous time
190   steps). In this study, we generalized the concept proposed by Nguyen et al. (2021) by allowing
191   the selection preference scheme to change continuously based on antecedent hydrologic
192   conditions (Equation 5). The temporal changes in the parameters of the beta function are
193   expressed as follows:

194   $$beta(P_S, a, b) = \frac{\Gamma(a+b)}{\Gamma(a) \cdot \Gamma(b)} \cdot P_S^{a-1} \cdot (1 - P_S)^{b-1} \tag{3}$$

195
$$r(t) = \frac{\int_{t-n}^{t} J(t) \cdot dt}{\int_{t-n}^{t} Q(t) \cdot dt} \tag{4}$$

196
$$a = \frac{\alpha}{r(t)} \tag{5}$$

197
$$b = \beta \cdot r(t) \tag{6}$$

198 where $beta(P_S, a, b)$ is the beta function with two positive shape parameters a [-] and b [-], Γ is
199 the gamma function, $r(t)$ [-] is the ratio between inflow and outflow to the SAS compartment
200 during the time $[t - n, \ t]$, n [T] is the time window to account for antecedent hydrologic
201 conditions, $Q(t)$ [L^3T^{-1}] is the outflow from the SAS compartment at time t, and α [-] and β [-]
202 are time-invariant parameters that control the rate of change of a and b with $r(t)$. In this
203 approach, α, β, and n are model parameters ($\alpha, \beta, n > 0$). Equations (4-6) show that an increase
204 in $r(t)$ will result in a decrease in a and an increase in b, indicating a stronger preference for
205 younger water. This reflects that an increase in $r(t)$ represents an increase in catchment storage
206 (or wetness), leading to the selection of younger water from storage. Compared to previous
207 approaches (Nguyen et al., 2021; van der Velde et al., 2015), this approach does not restrict the
208 parameter range of the beta function, allowing for all selection preference schemes that the beta
209 function could represent.

210 ### 2.3. Study area and data

211 The study area is the Selke catchment located in the northeastern Harz Mountains,
212 Germany. The Selke catchment has an area of about 457 km^2 with diverse landscapes and
213 hydrogeological settings (Figure 2a-d). The catchment consists of both lowland and mountainous
214 areas with elevation ranging between 106 m and 592 m above mean sea level (a.m.s.l) (Figure
215 2a). In the mountainous part, agricultural lands are patchy. The lowland areas are characterized
216 by extensive agricultural land use (Figure 2b). Both soil and geological maps show that the
217 mountainous areas are less heterogeneous than the lowland areas (Figure 2c-d). In the
218 mountainous areas (steeper slope), cambisols with high permeability overlaying low permeable
219 schist and claystone layers result in predominantly shallow flow paths (Jiang et al., 2014). In the
220 lowland areas (mild slope), chernozems with low permeability overlaying sedimentary deposit
221 layers allow for the development of deeper flow paths. The mountainous areas have shallower
222 aquifers compared to the lowland areas with deeper aquifers.

223 Table 1. Information about the upper, middle, and lower Selke subcatchments.

Subcatchment	upper Selke	middle Selke	lower Selke
Outlet gauge	Silberhütte	Meisdorf	Hausneindorf
Area (km^2 and % catchment area)	100.9 (22.1%)	78.9 (17.2%)	277.6 (60.7%)
Forest (% subcatchment area)	61.5	87.5	12.1
Agriculture (% subcatchment area)	36.0	10.2	75.8
Average elevation (m a.m.s.l)	448.9	370.0	164.8
Average slope (%)	6.8	11.5	2.6
Dominant soil types	Dystric/spodic cambisols		Haplic chernozems
Dominant geological units	Mississippian wacke/shale		Sedimentary material
Annual average precipitation (mm/year) (data from 2012-2019)	515.6	457.5	432.5
Average annual contribution to total catchment discharge (%)	50	25	25

224   Based on the distinct catchment characteristics and to make use of the observed data from
225   the three gauging stations (Silberhütte, Meisdorf, and Hausneindorf) for model evaluation, we
226   delineated the Selke catchment into three subcatchments, namely the upper, middle, and lower
227   Selke (Figure 2). The upper Selke is a mixed agriculture-forest subcatchment with high altitude,
228   high average annual rainfall, steep slope, shallow aquifer, and shallow flow paths. The middle
229   Selke is a forest-dominated subcatchment with hydrogeological settings similar to the upper
230   Selke. The lower Selke is an agriculturally-dominated subcatchment with gentle topography
231   (mild slopes), deeper aquifers, and deep subsurface flow paths. Detailed information about these
232   subcatchments is presented in Table 1 (see also Figure 2 for the spatial arrangement of different
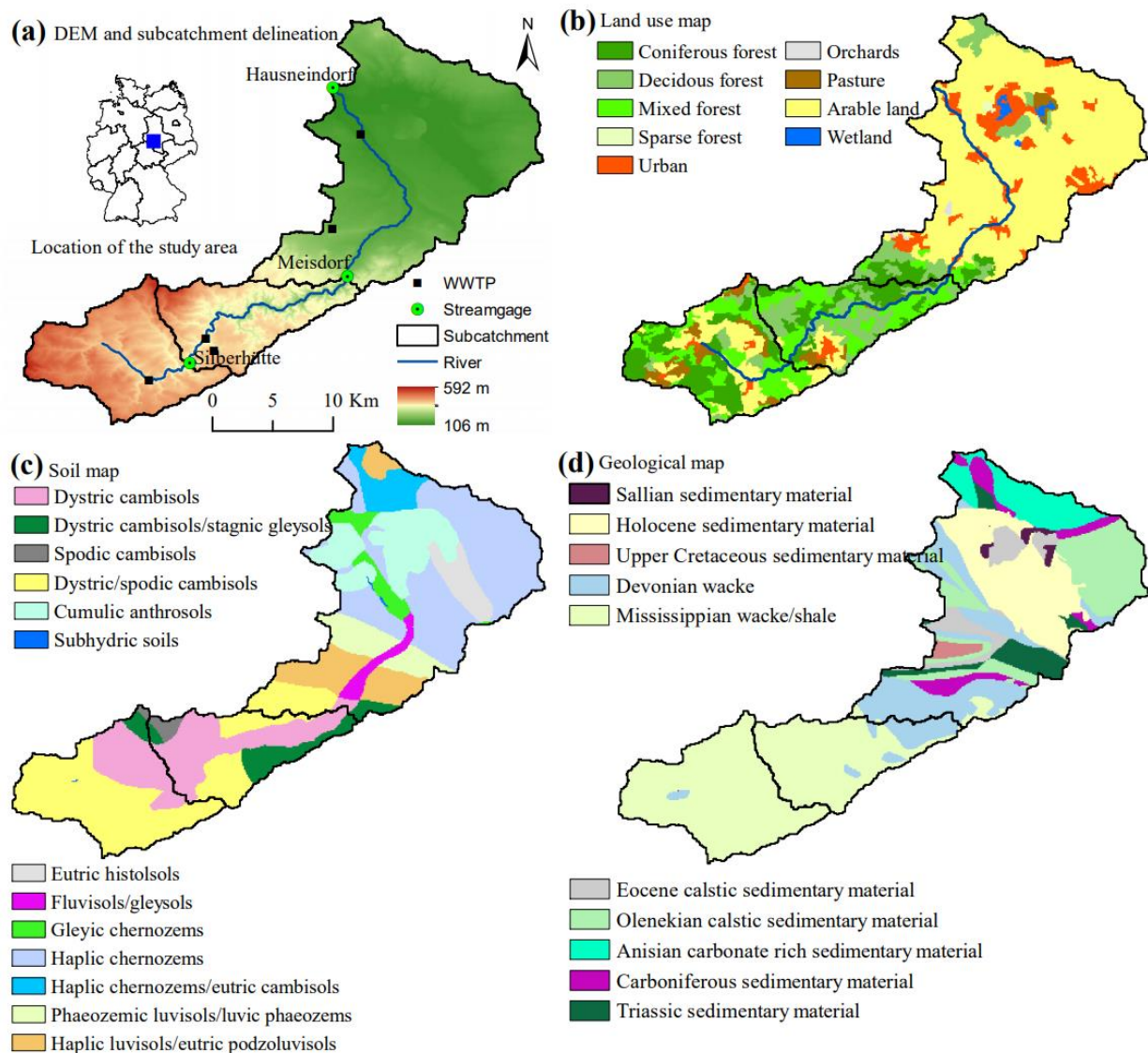233   landscape attributes).

234

235   **Figure 2**. Location of the study area and subcatchment delineation with (a) elevation, (b) land
236   use, (c) soil types, and (d) geological units.

237   In this study, model input and evaluation data were combined from different sources.
238   Daily precipitation, temperature, and potential evapotranspiration were provided by the German

239 Weather Service (DWD). Daily streamflow and instream nitrate concentration were obtained
240 from the State Office of Flood Protection and Water Management of Saxony-Anhalt (LHW) and
241 Helmholtz Center for Environmental Research (UFZ), respectively. Estimated nitrate load from
242 wastewater treatment plants (WWTP) as well as their locations were taken from X. Yang et al.,
243 (2018). Land use management practices (fertilizer, manure application, and crop rotation) are
244 based on field surveys and interviews (Yang et al., 2018). Other data (digital elevation model
245 (DEM), land use, soil, and geological map) were provided by the Federal Institute for
246 Geosciences and Natural Resources, Germany. Meteorological forcing constitutes of daily total
247 precipitation and average air temperature were acquired from the German Weather Service
248 (DWD). The point station data were gridded at a spatial resolution of 1×1 km^2 using the external
249 drift kriging interpolation approach with terrain elevation as an external variable (X. Yang et al.,
250 2018; Zink et al., 2017). The potential evapotranspiration was estimated with the Hargreaves &
251 Samani (1985) method.

252   2.4. Parameter sensitivity analysis

253   The objective of parameter sensitivity analysis is to identify the parameters (or processes)
254 that contribute most to the variability of streamflow and instream nitrate concentrations. This
255 information is further used to select parameters for optimization. The Elementary Effect Test
256 (EET, Campolongo et al., 2007; Morris, 1991) implemented in the Sensitivity Analysis For
257 Everybody (SAFE, Pianosi et al., 2015) toolbox was used for parameter sensitivity analysis. The
258 EET is an effective tool for screening non-influential parameters for models with a high number
259 of parameters (Campolongo et al., 2007; Pianosi et al., 2016). A further description of the EET is
260 presented in the supporting information (Text S1).

261   In this study, all global (catchment) and local (subcatchment-specific) parameters (M =
262 75 parameters) were selected for sensitivity analysis (Table S1). Global parameters are
263 catchment-scale parameters, while local parameters are SAS-related parameters that are defined
264 for each subcatchment. The parameter ranges were selected based on previous studies (Neitsch et
265 al., 2011; Nguyen et al., 2021; J. Yang et al., 2018; X. Yang et al., 2018) and parameter
266 distributions were assumed to be uniform. Parameter sensitivity analysis was carried out for the
267 period 2012-2019. All model runs were performed at a daily time step with a spatial resolution of
268 1 km^2. Detailed results of the parameter sensitivity analysis are shown in the supporting
269 information (Text S2 and Figure S1).

270   2.5. Parameter estimation and uncertainty analysis

271   In this study, parameters were optimized for the period 2012-2015 and validated for the
272 period 2015-2019 using observed streamflow and instream nitrate concentrations at the
273 Silberhütte, Meisdorf, and Hausneindorf gauging stations (Figure 2). Based on the results of
274 parameter sensitivity analysis, we selected the 21 most sensitive parameters (8 hydrological
275 parameters and 13 nitrate parameters) for optimization (Table 3, Text S2, and Figure S1). These
276 selected parameters include the different SAS-related parameters of all subcatchments, allowing
277 for the quantification of the uncertainty in the subsurface mixing and TTs.

278   For parameter optimization, we generated 400,000 parameter sets using the Latin
279 Hypercube Sampling (LHS) technique. LHS is an efficient approach for searching an ensemble
280 of optimal solutions, accounting for parameter uncertainties (Abbaspour et al., 2004; Sarrazin et
281 al., 2018). The same initial ranges of subsurface transport parameters ($\alpha, \beta,$ and k) in the three
282 subcatchments were used (Section 3.2). This means that we did not impose any prior knowledge

283   on subsurface mixing, water age, and denitrification conditions in these subcatchments. The
284   model prediction uncertainty was characterized by the 95 percent prediction uncertainty (95PPU)
285   band of behavioral simulations (Abbaspour et al., 2004). The lower and upper limits of the
286   95PPU band correspond to the 2.5% and 97.5% percentiles of the output variable at the
287   respective time step. The 95PPU band was evaluated by the *p* factor [0, 1] (the percentage of
288   measured data bracketed by the 95PPU band) and *r* factor [0, ∞) (the average thickness of the
289   95PPU band divided by the standard deviation of the measured data) (Abbaspour et al., 2004). In
290   general, higher *p* and lower *r* factors indicate lower prediction uncertainty.

291   The model performance was evaluated using the Nash–Sutcliffe Efficiency (*NSE*, Nash &
292   Sutcliffe, 1970), its logarithmic transformation (*lnNSE)*, and the bias (*BIAS)* (Text S3).
293   Behavioral simulations were selected using "soft rules" (e.g., Choi & Beven, 2007; Hartmann et
294   al., 2017; Sarrazin et al., 2018) by defining different threshold values for *NSE*, *lnNSE*, and *BIAS*
295   for streamflow (Q) and instream nitrate concentrations (C). This ensures that the simulated
296   results for both Q and C at all gauging stations meet a certain quality. The threshold values for
297   *NSE*, *lnNSE*, and *BIAS* were defined based on the simulated results, in a way that allows
298   uncertainty to be quantified (Hartmann et al., 2017), and are presented in the supporting
299   information (Text S3).

300   2.6. Evaluating the spatial model structure

301   Besides the aforementioned simulations (hereinafter referred to as simulation scenario 1:
302   base case), we performed additional simulation scenarios (SC 2 and SC 3; Table 2) to evaluate
303   the spatial model structure (semi-distributed and lumped SAS). Specifically, we determined
304   whether the subsurface transport parameters obtained from the lumped SAS approach
305   (catchment-scale SAS functions, SC 2) are applicable for the subcatchments, providing a similar
306   understanding of the subcatchment functioning as the semi-distributed SAS-based approach (SC
307   3). In the lumped SAS approach (SC 2), we conceptualized the entire subsurface of the Selke
308   catchment as a single storage compartment and applied the SAS concept to model nitrate export
309   from this compartment. For this evaluation, the lumped SAS model was calibrated at the
310   catchment outlet (Hausneindorf gauging station). The parameters selected for optimization were
311   based on the result of sensitivity analysis from the semi-distributed SAS model (SC 1, Table S2).
312   Then, the calibrated model parameters from the lumped approach (SC 2) were used for the
313   subcatchments (SC 3) to validate their applicability. In both semi-distributed (SC 1) and lumped
314   (SC2) SAS approaches, the same criteria were applied to select behavioral simulations.

315   Table 2. List of simulation scenarios. All simulation scenarios use the conceptual model as
316   shown in Figure 1 with the number of subcatchments varies from 1 to 3, depending on the
317   simulation scenario.

Simulation scenario (SC)	SAS approach (number of subcatchments)	Calibrated gauging station
SC1: base case	semi-distributed (3)	Silberhütte, Meisdorf, Hausneindorf
SC2: lumped SAS	lumped (1)	Hausneindorf
SC3: semi-distributed SAS	semi-distributed (3)	using calibrated parameters from SC 2

318

319   **3 Results and Discussion**

320   3.1. Streamflow, instream nitrate concentrations, and instream nitrate removal

321   Figure 3 shows the simulated streamflow and instream nitrate concentrations at the three
322   gauging stations from the base case scenario SC1 (Table 3). It can be seen that the model could
323   well capture the seasonality of streamflow and instream nitrate concentrations at the internal
324   gauging stations (Silberhütte and Meisdorf) as well as at the catchment outlet (Hausneindorf).
325   The model could represent high instream nitrate concentrations during the exceptional drought
326   years 2018 and 2019 (Hari et al., 2020), which were not part of the model calibration. However,
327   high flows are consistently underestimated by the model, which is a common issue with
328   hydrological models driven by daily meteorological forcing (e.g., Mizukami et al., 2019).

329   Statistical indices (the median *NSE*, *lnNSE*, and *BIAS*) show that the model performance
330   can be considered satisfactory (Figure S3a). In general, the model performance for the validation
331   period is slightly better than for the calibration period (except for instream nitrate concentrations
332   at the catchment outlet), indicating a slight underfitting in the calibration period. Considering
333   differences in hydrological conditions between the calibration and validation periods, in which
334   the validation period is drier with a multi-year drought period, the slight underfitting in the
335   calibration period is acceptable. The NSE for instream nitrate concentrations at the catchment
336   outlet during the calibration period is low due to the low seasonality of the observed data (Figure
337   3f or S3a). In this case, the NSE is high only if it can explain the short time-scale (e.g., daily)
338   fluctuations in the observed data (Schaefli & Gupta, 2007). Such short time-scale fluctuations
339   may be interpreted as noise in the data due to measurement/observational errors. Nevertheless,
340   other statistical indices, for example, the Kling-Gupta efficiency (KGE, Gupta et al., 2009) and
341   the correlation coefficient, indicate good model performance for instream nitrate concentrations
342   at the catchment outlet (Figure S3a). The r factors for instream nitrate concentrations (C) tend to
343   be higher than the r factors for streamflow (Q), indicating higher uncertainty for modeling
344   instream nitrate concentrations (Figure S3b). This is expected because the nitrate submodel is
345   affected by additional uncertainties in model structure and input data related to the agricultural
346   management practices. The p factors for both C and Q show that less than 60% of the observed
347   values are inside the 95PPU band. This is acceptable considering the narrow width of the 95PPU
348   band (reflected in small r factors) and strict criteria for *NSE*, *lnNSE*, and *BIAS* for behavioral
349   solutions (Text S3).

350   The results show that the instream nitrate removal rate is highly seasonal, namely high
351   during summer and low during winter (Figure S4). This is consistent with findings from previous
352   studies in the area (X. Yang et al., 2018). High instream nitrate removal rates during the drought
353   periods in 2018 and 2019 could be due to unusually high air/stream temperature and low-flow
354   conditions in these periods. Although the fraction of instream nitrate removal could be up to
355   about 50% during dry periods, the maximum cumulative instream nitrate removal among all
356   behavioral simulations for the entire simulation period (2012-2019) accounts for a maximum of
357   3% of the total nitrate export. The overall instream nitrate removal, however, could be significant
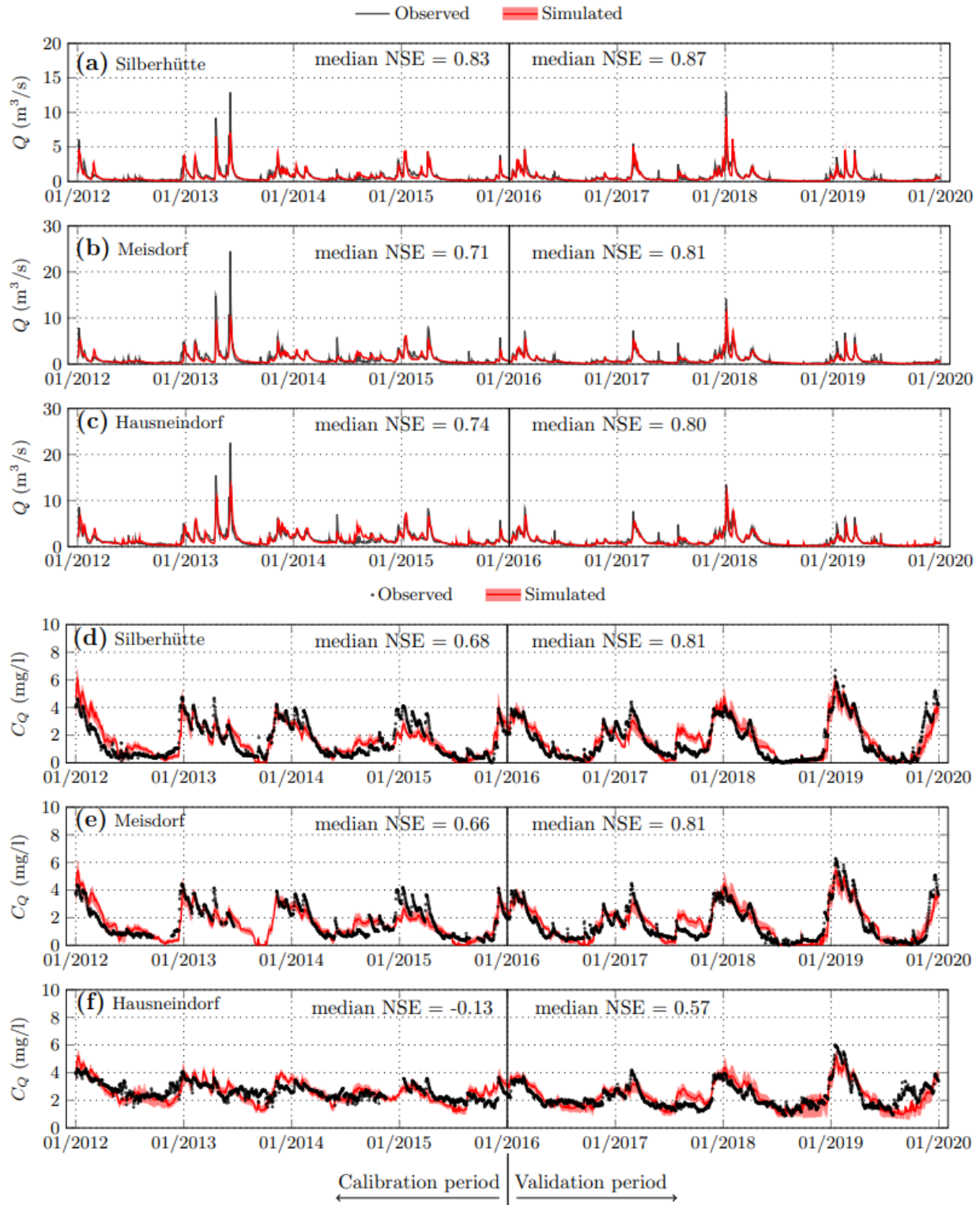358   for other areas (e.g., Alexander et al., 2000).

Figure 3. Simulated streamflow and instream nitrate concentrations at (a, d) the Silberhütte, (b, e) the Meisdorf, and (c, f) the Hausneindorf gauging stations in the base case scenario SC1. Solid lines indicate the median values, while bands indicate the 95PPU bands.

364   3.2. Behavioral parameter ranges

365   Statistical information about the behavioral parameter sets are shown in Table 3. Among
366 the calibrated parameters, only local parameters provide information about subcatchment
367 functioning. It is seen that the calibrated subsurface mixing parameters for upper (α_{up}, β_{up}) and
368 middle (α_{mid}, β_{mid}) Selke are in a similar and much narrower range, while those for the lower
369 Selke cover a wider ranges (Table 3). The denitrification rates in the upper (k_{up}) and middle
370 (k_{mid}) Selke are at least an order of magnitude higher compared to the denitrification rate in the
371 lower (k_{low}) Selke. Geochemical evidence from groundwater well data about subsurface
372 denitrification potential was reported for the upper and middle Selke; however, little to no sign of
373 subsurface denitrification in the lower Selke was found (Hannappel et al., 2018). Our model
374 results indicate similar subsurface mixing dynamics and reaction rates between the upper and
375 middle Selke, but different values for the lower Selke. This reflects similar hydrogeological
376 settings in the upper and middle Selke and the distinct hydrogeological setup of the lower Selke
377 (Figure 2). The behavioral ranges of α_{low} and β_{low} parameters in the lower Selke are not
378 significantly reduced compared to their initial ranges, indicating a relatively high uncertainty of
379 these parameters. Similar to previous works in the study area (Nguyen et al., 2021) and
380 elsewhere (Benettin et al., 2015, 2017), we found that using the observed streamflow and
381 instream solute concentrations is not sufficient to constrain the initial subsurface storage (Table
382 3).

383 Table 3. List of the selected parameters for optimization and the statistical characteristics of

384 behavioral parameter sets of the base case scenario SC1.

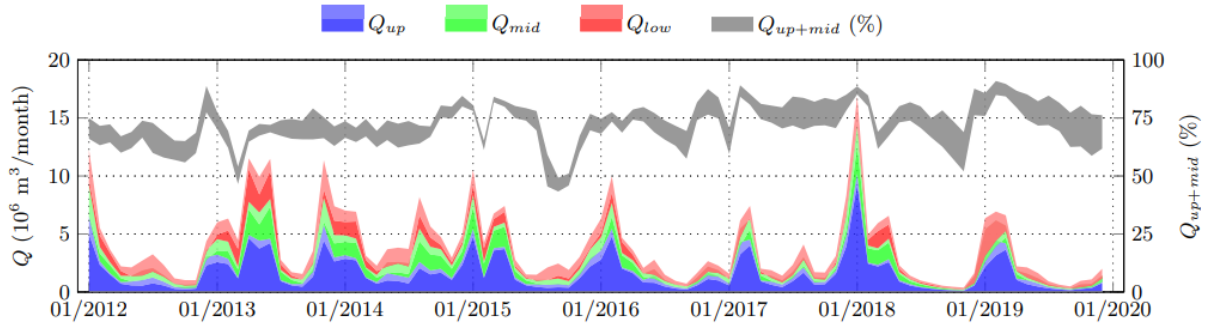| Parameter	Description	Initial range		Calibrated
		min	max	median [min, max]
Global (catchment-scale) parameter				
$soil_4$		0.65	0.95	0.78 [0.65, 0.95]
$soil_6$	Pedotransfer function parameters for soil hydrology routines of mHM	-0.37	-0.18	-0.32 [-0.37, -0.26]
$soil_7$		0.54	1.12	0.81 [0.57, 1.08]
$soil_9$		-0.55	-0.09	-0.27 [-0.55, -0.11]
$soil_{14}$	Fraction of roots in forest areas	0.90	0.99	0.98 [0.96, 0.99]
$soil_{17}$	Shape factor for calculating infiltration	1.00	4.00	2.49 [1.69, 3.23]
$runoff$	Direct surface runoff parameter	0.00	5.00	3.42 [0.08, 5.00]
pet_1	Correction factor for potential evapotranspiration	0.70	1.30	0.96 [0.92, 1.00]
k_{na}	Denitrification rate in nonagricultural soil (day^{-1})	1.00e-8	1.00e-1	1.00e-2 [4.13e-3, 2.42e-2]
k_a	Denitrification rate in agricultural soil (day^{-1})	1.00e-8	1.00e-1	2.18e-2 [5.68e-3, 4.11e-2]
k_{str}	Denitrification rate in the stream network (day^{-1})	1.00e-8	1.00e-3	2.72e-6 [3.07e-8, 2.76e-4]
C_0	Initial nitrate concentration in the subsurface (mg/L)	0.5	10.0	7.86 [4.43, 8.85]
Local (subcatchment-specific) parameter				
α_{up}	Parameters of the SAS function (upper Selke)	0.01	5.00	0.36 [0.10, 0.97]
β_{up}		0.01	5.00	4.28 [0.77, 4.84]
S_{0_up}	Initial subsurface storage of the upper Selke (mm)	500.00	5000.00	798.0 [565.0, 4959.9]

k_{up}	Subsurface denitrification rate in the upper Selke (day^{-1})	1.00e-8	1.00e-2	9.06e-3 [3.42e-3, 9.60e-3]
α_{mid}	Parameters of the SAS function (middle Selke)	0.01	5.00	0.44 [0.10, 1.29]
β_{mid}		0.01	5.00	3.29 [1.06, 4.00]
k_{mid}	Subsurface denitrification rate in the middle Selke (day^{-1})	1.00e-8	1.00e-2	1.05e-3 [3.01e-4, 7.87e-3]
α_{low}	Parameters of the SAS function (lower Selke)	0.01	5.00	1.84 [0.22, 4.78]
β_{low}		0.01	5.00	1.95 [0.12, 4.71]
k_{low}	Subsurface denitrification rate in the lower Selke (day^{-1})	1.00e-8	1.00e-2	4.96e-6 [3.43e-7, 8.40e-5]

385

386   3.3. Subcatchment discharge and nitrate export

387   Figure 4a shows the contribution of discharge from each subcatchment to the total
388 catchment discharge. Overall, the simulated results show that a dominant fraction of catchment
389 discharge (about 48-51% considering the 95PPU band) originates from the upper Selke although
390 it only accounts for 22.1% of the catchment area. The middle and lower Selke contribute a
391 comparable amount of discharge (23-25% and 24-29% of catchment discharge, respectively)
392 despite having significantly different areal percentages (17.2% and 61.7%, respectively). These
393 results are comparable with those obtained from observed data (Table 1). Although the fraction
394 of total discharge from the upper and middle Selke varies seasonally in a wide range, it remains
395 mostly above 50%, and thus constitutes a dominant source of catchment discharge even during
396 low-flow periods (Figure 4a).

397   In terms of exported nitrate load, the lower Selke contributes a substantial portion of
398 nitrate load (about 44-55%) despite its relatively low discharge contribution (Figure 4a-b). The
399 exported nitrate loads from the upper and middle Selke account for 31-38% and 13-18% of the
400 catchment nitrate export, respectively. During high-flow periods, the exported nitrate load from
401 the upper and middle Selke (predominantly the upper Selke) is much higher than that from the
402 lower Selke (Figure 4b). During low-flow periods, however, the lower Selke contributes the
403 major fraction of the catchment nitrate export. This is because during low-flow periods (1)
404 instream nitrate concentrations in discharge from the lower Selke are much higher than that from
405 the upper and middle Selke (Figure 4c), and (2) discharge contribution from the lower Selke
406 could increase up to 50%. The results also show that instream nitrate concentrations from the
407 upper and middle Selke have a clear seasonal pattern (high during high-flow and low during low-
408 flow periods), while that from the lower Selke is relatively stable (Figure 4c). This is related to
409 the differences in the subsurface mixing, transport time, and denitrification timescale (Section
410 3.4). The uncertainty in the simulated nitrate concentrations in discharge from the lower Selke is
411 relatively large during low-flow periods in 2012, 2016, and 2018 compared to other periods
412 (Figure 4c). This is due to the uncertainty in the estimated nitrate concentrations in the oldest
413 water pool (or initial nitrate concentration C_0) and the interplay between denitrification and
414 transport timescales (Section 3.4)

(a) Subcatchment discharge

(b) Subcatchment nitrate export (load)

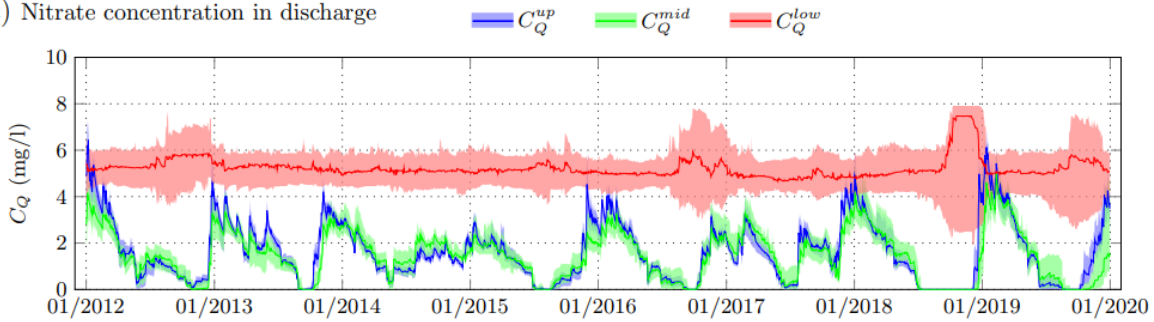**(c)** Nitrate concentration in discharge

Figure 4. Contribution of (a) discharge Q, (b) exported nitrate load L_{N-NO_3}, and (c) nitrate concentrations in discharge C_Q from individual subcatchments (scenario SC1). The superscripts "*up*", "*mid*", and "*low*" indicate the upper, middle, and lower Selke, respectively. Discharge and exported nitrate load were aggregated from daily to monthly for better visualization. Light (blue, red, and green) color bands in (a)-(c) and grey band in (a)-(b) indicate the 95PPU bands from behavioral simulations, darker (blue, red, green) color bands in (a)-(c) indicate the area (volume of discharge, and mass of nitrate) under the 95PPU bands, and solid lines in (a)-(c) indicate the median values.

The reliability of the simulated nitrate concentrations in discharge from the middle Selke (Figure 4c) is lower compared to that from the upper Selke. This is because most of the nitrate at the Meisdorf gauging station originates from the upper Selke, so the nitrate concentration data at the Meisdorf gauge do not contain much additional information for the model calibration. Considering the aforementioned reason and the comparable instream dynamics (Figure 4c) as well as the behavioral subsurface parameter ranges (Table S2) between the upper and middle

430   Selke, those subcatchments could be considered as one subcatchment for future studies.

431   3.4. Linking subsurface mixing with water age and nitrate export

432   Figure 5 shows the relation between subsurface mixing and the TTs of discharge as well
433   as nitrate export from the three subcatchments. The upper Selke tends to select young water (a/b
434   < 1 in Eqs. 4-7) for discharge, apart from low-flow periods (a/b > 1; Figure 5a). The catchment
435   progressively shifts from young (or old) to old (or young) water selection preference with
436   decreasing wetness. The selection preference for young water during high-flow periods is
437   consistent with our understanding that fast shallow flow paths dominate under these flow
438   conditions. These flow paths can be activated due to a combination of 1) high precipitation, 2)
439   high permeability of the uppermost cambisols layer, and 3) low percolation rate of the lower
440   schist and claystone layers (Section 2.3 and Figure 2c). During low-flow periods, we found a
441   dominance of old water in the simulated discharge, causing a strong difference in the TTs of
442   discharge between high and low-flow periods (Figure 5b). This can be explained by the fact that
443   the relative contribution of discharge from deeper and longer flow paths to streamflow becomes
444   more pronounced in low-flow periods, because less flow from the shallower zone with shorter
445   flow paths is generated when those shallow flow paths increasingly cease. It should be noted that
446   the maximum TT is rather restricted by the time frame of the simulation rather than the actual
447   age of the oldest water, which is unknown (Figure 5b). Discharge with older water has less
448   nitrate compared to discharge with younger age due to longer time for denitrification, creating a
449   pronounced seasonality in instream nitrate concentrations (Figure 5b). In addition, the
450   seasonality in instream nitrate concentrations is also due to the seasonality of nitrate
451   concentrations in the percolation water (Figure 5b). However, due to denitrification and
452   subsurface mixing, the range of nitrate concentrations in discharge is buffered compared to that
453   in the percolating water.

454   The middle Selke shows a similar behavior to the upper Selke in terms of subsurface
455   mixing and nitrate export dynamics (Figure S5). In addition, the subsurface denitrification rates
456   in the upper and middle Selke are comparable (Table 3). This is expected because the upper and
457   middle Selke have similar hydrogeological settings (Table 1 and Figure 2). Visual assessment
458   shows that the model prediction uncertainties (the 95PPU of a/b, TT_{50}, and C_Q) for the middle
459   Selke tend to be higher than that for the upper Selke (Figures S4) for the reason mentioned
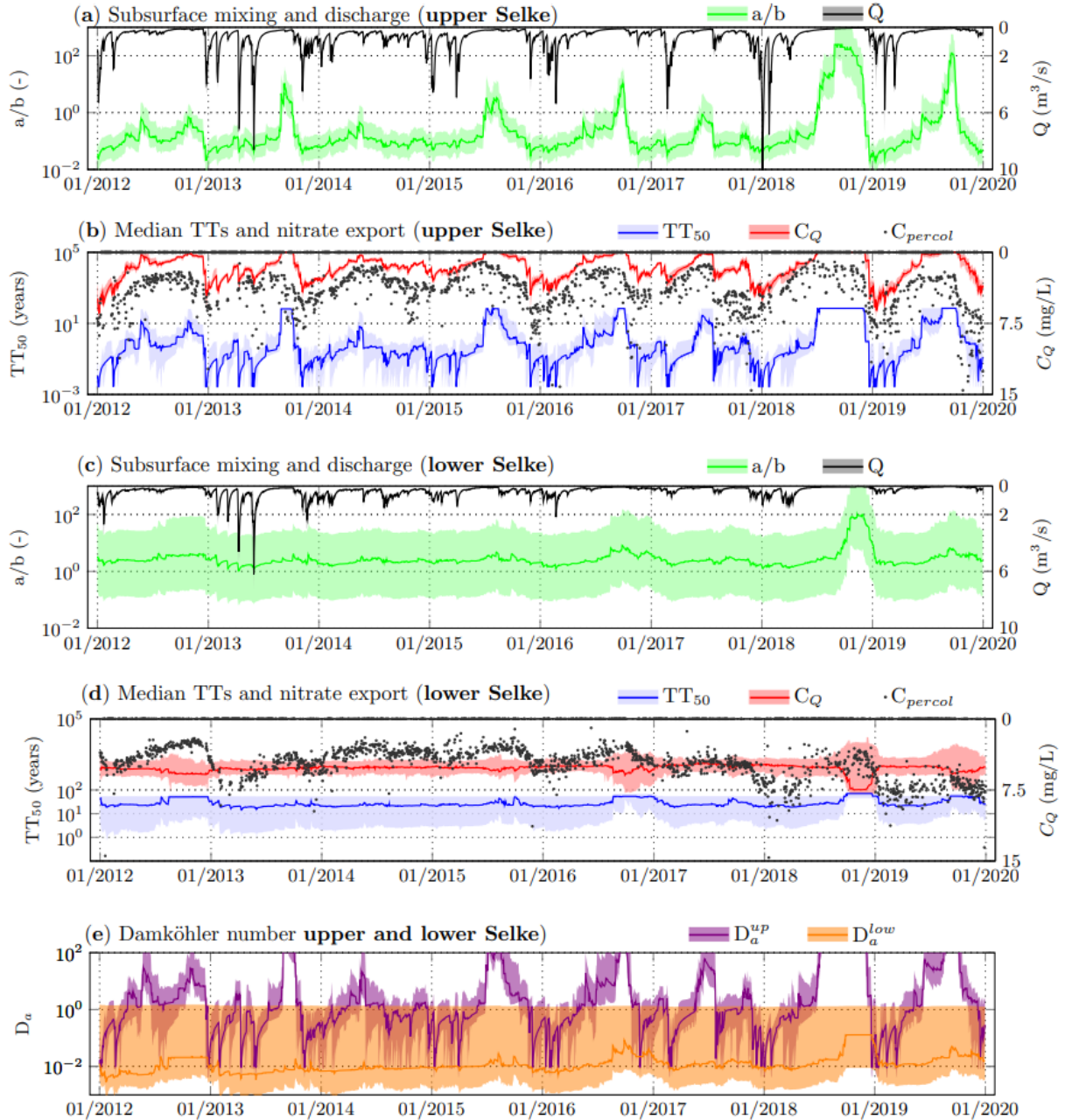460   earlier (Section 3.3).

461

Figure 5. Relation between subsurface mixing dynamics (characterized by the *a/b* ratio of the beta function), TTs (characterized by the median transit time TT_{50}), and nitrate concentration dynamics in discharge (C_Q) from (a-b) the upper Selke and (c-d) the lower Selke, and (e) the interplay between transport time and denitrification timescale (characterized by the Damköhler number, D_a) in the upper and lower Selke. Solid lines indicate the median values, while bands indicate the 95PPU band. The superscripts "*up*" and "*low*" mean the upper and lower Selke, respectively. C_{percol} is the nitrate concentration in percolated water. The Damköher number is the ratio between TT_{50} of discharge and the reaction time (*1/k*). Results are from individual subcatchments.

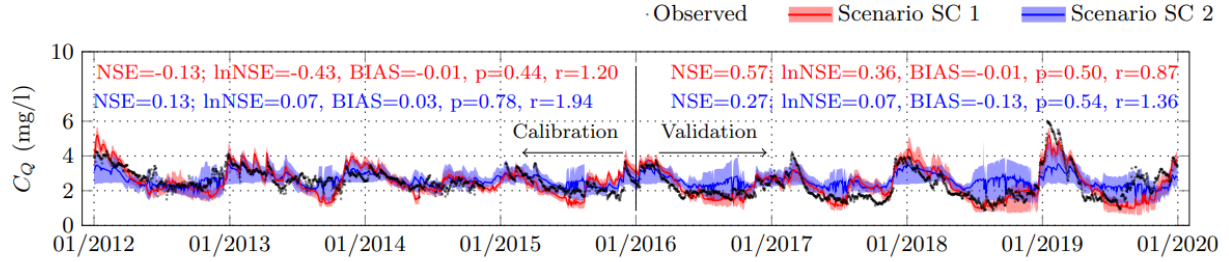Compared to the upper and middle Selke, the selection preference for discharge (*a/b*

472 ratio) in the lower Selke varies over a smaller range (Figures 5a,c and S5b). This is to be
473 expected considering that the lower Selke has smaller topographic gradients (flatter terrain) and a
474 deeper aquifer system with more steady, less dynamic subsurface flow field (Nixdorf & Trauth,
475 2018; J. Yang et al., 2018). The median *a/b* ratio shows that subsurface mixing in the lower
476 Selke varies around the complete mixing ratio (*a/b* = 1) except during the very dry periods in
477 which the system discharges only old water. As a result, the TTs of discharge from the lower
478 Selke are much higher than those from the upper and middle Selke, which preferably discharge
479 young water most of the time (Figures 5a,c and S5b). The relation between nitrate concentrations
480 in discharge and TTs of discharge from the lower Selke is unclear, as nitrate concentrations in
481 discharge from the lower Selke seem to be relatively steady throughout the years (Figure 5d).
482 This is because subsurface mixing in the lower Selke (Figure 5c) is relatively stable around an
483 a/b ratio of 1, which describes complete mixing behavior. Interestingly, the median subsurface
484 transport time in the lower Selke subcatchment is faster compared to the denitrification timescale
485 defined by the very low denitrification rate (Figure 5e, Table 3). During low-flow periods, the
486 initial nitrate concentration in the oldest water pool has negligible impacts on the nitrate export
487 from the upper Selke compared to that from the lower Selke (Figure 5b,d). This is because the
488 upper Selke during those periods is characterized by relatively long subsurface transport times
489 compared to the denitrification timescale so that denitrification is controlled by the high
490 denitrification rates and most nitrate is removed along the deeper flow paths. In contrast, in the
491 lower Selke subsurface transport times, although generally longer than in the upper Selke, are
492 short relative to the very long reaction time scales caused by the very low denitrification rates,
493 making the system transport-controlled as indicated by the D_a numbers during low-flow periods
494 (Figure 5e). In general, subsurface transport in the upper Selke is characterized by a strong
495 variability of transport time-scales over the denitrification timescale (shown by the D_a numbers,
496 Figure 5e), while subsurface transport in the lower Selke is more steady and characterized by
497 transport time scales that are shorter than the respective reaction time scales.

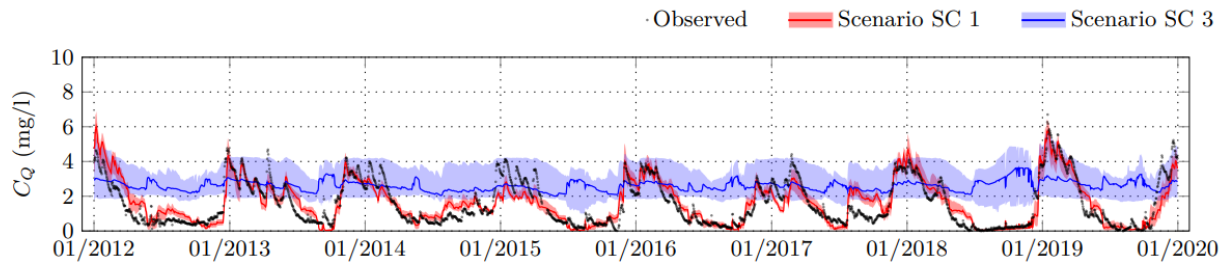498   3.5. Semi-distributed versus lumped SAS approach

499   Comparing results from the semi-distributed (SC 1) and lumped (SC 2) SAS approaches
500 show that model performances for instream nitrate concentrations at the catchment outlet are
501 somewhat different (Figure 6a). The median statistical indices (*NSE* and *lnNSE*) indicate that the
502 lumped approach calibrated with data from the catchment outlet only has a better model
503 performance than the semi-distributed approach in the calibration period (Figure 6a). The
504 slightly poorer model performance of the semi-distributed model, despite having higher degrees
505 of freedom, is because the semi-distributed SAS model is constrained with streamflow and
506 instream nitrate concentration data not only from the catchment outlet, but also from the internal
507 gauging stations (Table 2). In the validation period, however, it can be seen clearly that the semi-
508 distributed approach performs significantly better than the lumped approach. This suggests that
509 the dynamics of age selection for discharge and the associated turnover of nitrate are indeed
510 distinctly different between the three sub-catchments and cannot be adequately represented with
511 the simpler lumped approach. A better model performance in the calibration period with the
512 lumped approach could be an artifact of the optimization. In fact, a misrepresentation of three
513 SAS functions by one SAS function can be compensated by other non-SAS-related parameters in
514 the calibration period but not in the validation period. The results further suggest that for model
515 applications beyond the calibration period (e.g., climate change and land-use change impact
516 studies), the semi-distributed approach should be preferred over the lumped approach. For
517 streamflow simulation, the two approaches have comparable results with median NSE values

518   from both approaches being within the range [0.73, 0.89] for both calibration and validation
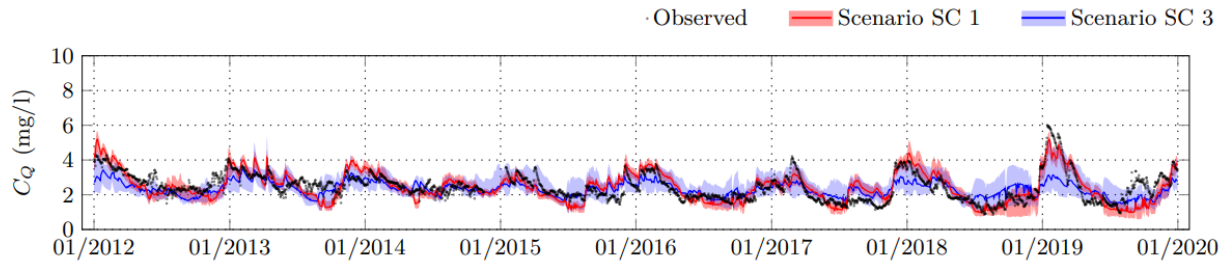519   periods (not shown).

520

Figure 6. Observed and simulated (a, c) instream nitrate concentrations at the catchment outlet
(Hausneindorf) and (b) the internal gauging station (Silberhütte) from different simulation
scenarios (Table 2). Solid lines indicate the median values, while bands indicate the 95PPU
band.

526   Next, we compared the simulations of nitrate dynamics based on the semi-distributed and
527   lumped SAS approaches to understand how well the internal catchment functioning can be
528   represented with spatially lumped SAS functions. Figure 6b-c shows the simulated instream
529   nitrate concentrations at the internal gauging station (e.g., Silberhütte) and the catchment outlet
530   (Hausneindorf) using the calibrated catchment-scale subsurface parameters (α, β, n, S_0) obtained
531   from the lumped approach for all subcatchments (SC 3). It is clearly visible that these parameters
532   cannot be used for the subcatchments as they provide a false understanding of the subcatchment
533   functioning (Figure 6b). For example, the simulated nitrate concentrations in discharge from the
534   upper Selke (SC 3) are relatively high and steady throughout the years, while those from the
535   observed data and the semi-distributed SAS approach (SC 1) show a strong seasonality (Figures
536   6b). The relatively steady simulated nitrate concentrations in discharge (SC 3) are due to (1)

537 faster TTs and higher nitrate concentrations in young water (percolated water) during high-flow
538 periods and (2) longer TTs and high nitrate concentration in the old water pool due to the very
539 low denitrification rate during low-flow periods (Figure S6 and Table S2). In the dry periods, the
540 simulated nitrate concentrations (SC 3) are even slightly higher than those in the high-flow
541 periods (e.g., during 2018-2019; Figure 6b), suggesting contrasting catchment functioning
542 compared to observed data and results from the semi-distributed approach (SC 1). The simulated
543 subsurface mixing and TT dynamics from the upper Selke (SC 3) indicate that using parameters
544 from the lumped approach (SC 2) will shift the selection preference for discharge to much older
545 water compared to the semi-distributed approach (SC 1) (Figure S6).

546 Despite a clear mismatch at the internal gauging station, the simulated instream nitrate
547 concentrations at the catchment outlet match quite well the observations (Figure 6c). This
548 indicates that taking the same subsurface transport parameters for all subcatchments in a highly
549 heterogeneous catchment could provide the right results at the catchment outlet for the wrong
550 reasons. For spatially explicit SAS models, this means that a parameter regionalization technique
551 could be needed to parameterize the subsurface transport parameters of each spatial modeling
552 unit (e.g., sub-catchments or HRUs or grid-cells) to be applicable in heterogeneous catchments,
553 thus assisting (land use) management decisions.

554 Results from the lumped and semi-distributed models also imply that if the lower Selke is
555 further divided into smaller modeling units, individual responses from these modeling units can
556 be different from the integrated response of the lower Selke. This is because the geological
557 setting of the lower Selke is highly heterogeneous (Figure 2d). In this case, additional data
558 (internal gauging stations) are required for further understanding the internal functioning of
559 different modeling units within the lower Selke. However, further discretization of the upper and
560 middle Selke into smaller modeling units might not change our understanding of the internal
561 subcatchment functioning, as the soil and geological conditions in these areas are quite
562 homogeneous. Therefore, the responses of these smaller modeling units are expected to be
563 similar (as shown by the similar responses of the upper and lower Selke; Section 3.4).

564 4 Model capabilities, implications for management practices, and limitations

565 This study demonstrated that the spatially explicit (e.g., semi-distributed) SAS approach
566 can provide valuable additional insights into the functioning of each subcatchment with
567 internally consistent process descriptions, while at the same time it does not compromise the
568 quality of the model fit at the integral point of the main catchment outlet. In contrast, the lumped
569 SAS approach could only yield robust results at the main catchment outlet and yielded
570 inadequate results at internal points in the model domain. Our application of the semi-distributed
571 SAS model in a nested mesoscale heterogeneous catchment has demonstrated the model's ability
572 to capture nitrate dynamics at internal gauging stations as well as at the main catchment outlet.
573 Applying SAS functions in a semi-distributed framework as presented here, helps to overcome
574 some of the limitations of the spatially lumped characteristics of the general SAS concept.
575 Results from a semi-distributed model can provide not only additional spatial information, such
576 as subcatchment nitrate export, but also temporal information on the age of water and potentially
577 nitrate, which is) related to the source and origin of the exported nitrate.

578 The spatially explicit SAS approach is especially relevant for planning and evaluating
579 spatial management practices as (1) parameters infer from the lumped approach could fail to
580 represent the subcatchment functioning, (2) the lumped approach is less robust than the semi-

581   distributed approach, and (3) the lumped approach does not provide information about both
582   spatial and temporal origins of nitrate in discharge for effective management. Results from the
583   Selke with the semi-distributed SAS approach show that the lowland catchments (lower Selke)
584   should have different management practices compared to the mountainous headwater catchments
585   (middle and upper Selke). Agricultural management practices that aim to quickly reduce nitrate
586   export during high-flow periods should be implemented in the mountainous headwater
587   catchments rather than in the lowland catchment. This is because of the short TTs and transport-
588   limited characteristics of these catchments during high-flow periods. However, management
589   practices that aim to reduce exported nitrate loads (1) during low-flow periods or (2) in the
590   coming decade(s) should be implemented in the lowland catchments with longer TTs and
591   transport-limited characteristics. Due to the short median TTs in the mountainous catchments (~
592   1 year), the effectiveness of management practices in these catchments can be evaluated in the
593   following years. In contrast, long median TTs in the lowland catchment would require decades
594   for the effects of a certain management practice to become effective and visible.

595   Despite the advantages of the semi-distributed SAS approach, the application of this
596   approach in larger catchments with more diverse hydrogeological settings could face several
597   challenges. In such catchments, the number of subsurface parameters could be high due to a high
598   number of subcatchments. In this case, understanding the linkage between key catchment
599   characteristics (e.g., topography, geology, land use, and meteorological conditions) with
600   subcatchment functioning (parameters of the SAS function) could avoid unnecessary small
601   spatial resolution and model overparameterization. This can provide useful insights into the
602   optimal spatial modeling resolution, in which the number of modeling units is at a minimum
603   while the spatial heterogeneity of subcatchment responses is adequately captured. For such
604   understanding, applications of the semi-distributed SAS approach in much larger catchments
605   with diverse settings are required.

606

5 Conclusions

608   In this study, we developed a semi-distributed SAS-based model, in which SAS functions
609   are applied at the subcatchment level. The proposed model was applied in a mesoscale nested
610   catchment, namely the Selke catchment located in Germany. The catchment was delineated into
611   three subcatchments for application of SAS functions, consisting of (1) a upper mountainous
612   headwater subcatchment (upper Selke) with a mixture of forest and agricultural land, (2) a
613   middle mountainous subcatchment (middle Selke) dominated by forest land, and (3) a lowland
614   subcatchment (lower Selke) dominated by agricultural land. The main results from this study are
615   as follows:

616   • The semi-distributed SAS approach could represent instream nitrate concentration
617   dynamics not only at the catchment outlet but also at the internal gauging stations.

618   • The headwater subcatchment has high seasonal variations in the subsurface mixing
619   schemes, while that in the lowland catchment is less pronounced. Nitrate concentrations
620   in discharge from the headwater subcatchment show a strong seasonality, while those
621   from the lowland subcatchment are relatively steady over different seasons.

622   • Instream denitrification only removes a minor part of the exported nitrate loads.

623   • The median age of water in discharge (TT_{50}) from the headwater subcatchment is much

624   younger than that from the lowland subcatchment.

625   • The headwater and lowland subcatchments take turns at dominating catchment nitrate
626   export in high and low-flow periods.

627   • Parameters infer from the lumped approach fail to represent the subcatchment
628   functioning and the lumped approach is less robust than the semi-distributed approach

629   Results from this study have demonstrated that the proposed model can provide useful
630 insights into the functioning of each subcatchment, unlike the lumped SAS approach. The
631 proposed model concept in combination with an appropriate regional parameterization approach
632 could help to extend the application of the SAS concept in larger catchments. Results from such
633 model applications could help understand both spatial and temporal origins of nitrate in rivers,
634 contributing towards efforts to reduce nitrate pollution.

References

Abbaspour, K. C., Johnson, C. A., & van Genuchten, M. T. (2004). Estimating Uncertain Flow and Transport Parameters Using a Sequential Uncertainty Fitting Procedure. *Vadose Zone Journal*, *3*(4), 1340–1352. https://doi.org/10.2136/vzj2004.1340

Alexander, R. B., Smith, R. A., & Schwarz, G. E. (2000). Effect of stream channel size on the delivery of nitrogen to the Gulf of Mexico. *Nature*, *403*(6771). https://doi.org/10.1038/35001562

Benettin, P., & Bertuzzo, E. (2018). Tran-SAS v1.0: A numerical model to compute catchment-scale hydrologic transport using StorAge Selection functions. *Geoscientific Model Development*, *11*(4), 1627–1639. https://doi.org/10.5194/gmd-11-1627-2018

Benettin, P., Kirchner, J. W., Rinaldo, A., & Botter, G. (2015). Modeling chloride transport using travel time distributions at Plynlimon, Wales. *Water Resources Research*. https://doi.org/10.1002/2014WR016600

Benettin, P., Soulsby, C., Birkel, C., Tetzlaff, D., Botter, G., & Rinaldo, A. (2017). Using SAS functions and high-resolution isotope data to unravel travel time distributions in headwater catchments. *Water Resources Research*. https://doi.org/10.1002/2016WR020117

Benettin, P., Van Der Velde, Y., Van Der Zee, S. E. A. T. M., Rinaldo, A., & Botter, G. (2013). Chloride circulation in a lowland catchment and the formulation of transport by travel time distributions. *Water Resources Research*, *49*(8), 4619–4632. https://doi.org/10.1002/wrcr.20309

Boeykens, S. P., Piol, M. N., Samudio Legal, L., Saralegui, A. B., & Vázquez, C. (2017). Eutrophication decrease: Phosphate adsorption processes in presence of nitrates. *Journal of Environmental Management*, *203*. https://doi.org/10.1016/j.jenvman.2017.05.026

Botter, G., Bertuzzo, E., & Rinaldo, A. (2011). Catchment residence and travel time distributions: The master equation. *Geophysical Research Letters*, *38*(11), 1–6. https://doi.org/10.1029/2011GL047666

Breuer, L., Vaché, K. B., Julich, S., & Frede, H. G. (2008). Current concepts in nitrogen dynamics for mesoscale catchments. *Hydrological Sciences Journal*, *53*(5). https://doi.org/10.1623/hysj.53.5.1059

Buzacott, A. J. V., van der Velde, Y., Keitel, C., & Vervoort, R. W. (2020). Constraining water age dynamics in a south-eastern Australian catchment using an age-ranked storage and stable isotope approach. *Hydrological Processes*. https://doi.org/10.1002/hyp.13880

Campolongo, F., Cariboni, J., & Saltelli, A. (2007). An effective screening design for sensitivity analysis of large models. *Environmental Modelling and Software*, *22*(10). https://doi.org/10.1016/j.envsoft.2006.10.004

Choi, H. T., & Beven, K. (2007). Multi-period and multi-criteria model conditioning to reduce prediction uncertainty in an application of TOPMODEL within the GLUE framework. *Journal of Hydrology*, *332*(3–4). https://doi.org/10.1016/j.jhydrol.2006.07.012

Cunge, J. A. (1969). On the subject of a flood propagation computation method (Muskingum method). *Journal of Hydraulic Research*. https://doi.org/10.1080/00221686909500264

Dupas, R., Ehrhardt, S., Musolff, A., Fovet, O., & Durand, P. (2020). Long-term nitrogen retention and transit time distribution in agricultural catchments in western France. *Environmental Research Letters*, *15*(11). https://doi.org/10.1088/1748-9326/abbe47

Ebeling, P., Kumar, R., Weber, M., Knoll, L., Fleckenstein, J. H., & Musolff, A. (2021). Archetypes and Controls of Riverine Nutrient Export Across German Catchments. *Water Resources Research*, *3*, 1–29. https://doi.org/10.1029/2020wr028134

Ehrhardt, S., Kumar, R., Fleckenstein, J. H., Attinger, S., & Musolff, A. (2019). Trajectories of nitrate input and output in three nested catchments along a land use gradient. *Hydrology and Earth System Sciences*, *23*(9), 3503–3524. https://doi.org/10.5194/hess-23-3503-2019

European Commission. (2018). Report from the commission to the council and the European Parliament on the implementation of Council Directive 91/676/EEC concerning the protection of waters against pollution caused by nitrates from agricultural sources based on Member State reports fo. *European Commission*.

European Environment Agency. (2012). *EEA Catchments and Rivers Network System ECRINS v1.1 - Rationales, building and improving for widening uses to Water Accounts and WISE applications* (Issue 7).

Gupta, H. V., Kling, H., Yilmaz, K. K., & Martinez, G. F. (2009). Decomposition of the mean squared error and NSE performance criteria: Implications for improving hydrological modelling. *Journal of Hydrology*, *377*(1–2). https://doi.org/10.1016/j.jhydrol.2009.08.003

Hannappel, S., Köpp, C., & Bach, T. (2018). Characterization of the denitrification potential of aquifers in Saxony-Anhalt. *Grundwasser*, *23*(4), 311–321. https://doi.org/10.1007/s00767-018-0402-7

Hargreaves, G. H., & Samani, Z. A. (1985). Reference Crop Evapotranspiration from Temperature. *Applied Engineering in Agriculture*, *1*(2). https://doi.org/10.13031/2013.26773

Hari, V., Rakovec, O., Markonis, Y., Hanel, M., & Kumar, R. (2020). Increased future occurrences of the exceptional 2018–2019 Central European drought under global warming. *Scientific Reports*. https://doi.org/10.1038/s41598-020-68872-9

Harman, C. J. (2015). Time-variable transit time distributions and transport: Theory and application to storage-dependent transport of chloride in a watershed. *Water Resources Research*. https://doi.org/10.1002/2014WR015707

Harman, C. J. (2019). Age-Ranked Storage-Discharge Relations: A Unified Description of Spatially Lumped Flow and Water Age in Hydrologic Systems. *Water Resources Research*, *55*(8), 7143–7165. https://doi.org/10.1029/2017WR022304

Hartmann, A., Antonio Barberá, J., & Andreo, B. (2017). On the value of water quality data and informative flow states in karst modelling. *Hydrology and Earth System Sciences*, *21*(12). https://doi.org/10.5194/hess-21-5971-2017

Hrachowitz, M., Benettin, P., van Breukelen, B. M., Fovet, O., Howden, N. J. K., Ruiz, L., van der Velde, Y., & Wade, A. J. (2016). Transit times-the link between hydrology and water quality at the catchment scale. *Wiley Interdisciplinary Reviews: Water*, *3*(5), 629–657. https://doi.org/10.1002/wat2.1155

726 Jiang, S., Jomaa, S., & Rode, M. (2014). Modelling inorganic nitrogen leaching in nested
727   mesoscale catchments in central Germany. *Ecohydrology*, *7*(5), 1345–1362.
728   https://doi.org/10.1002/eco.1462

729 Knobeloch, L., Salna, B., Hogan, A., Postle, J., & Anderson, H. (2000). Blue babies and nitrate-
730   contaminated well water. *Environmental Health Perspectives*.
731   https://doi.org/10.1289/ehp.00108675

732 Knoll, L., Breuer, L., & Bach, M. (2019). Large scale prediction of groundwater nitrate
733   concentrations from spatial data using machine learning. *Science of the Total Environment*,
734   *668*, 1317–1327. https://doi.org/10.1016/j.scitotenv.2019.03.045

735 Kumar, R., Samaniego, L., & Attinger, S. (2013). Implications of distributed hydrologic model
736   parameterization on water fluxes at multiple scales and locations. *Water Resources
737   Research*. https://doi.org/10.1029/2012WR012195

738 Lassaletta, L., García-Gómez, H., Gimeno, B. S., & Rovira, J. V. (2009). Agriculture-induced
739   increase in nitrate concentrations in stream waters of a large Mediterranean catchment over
740   25 years (1981-2005). *Science of the Total Environment*, *407*(23).
741   https://doi.org/10.1016/j.scitotenv.2009.08.002

742 Lindström, G., Pers, C., Rosberg, J., Strömqvist, J., & Arheimer, B. (2010). Development and
743   testing of the HYPE (Hydrological Predictions for the Environment) water quality model
744   for different spatial scales. *Hydrology Research*. https://doi.org/10.2166/nh.2010.007

745 Mizukami, N., Rakovec, O., Newman, A. J., Clark, M. P., Wood, A. W., Gupta, H. V., & Kumar,
746   R. (2019). On the choice of calibration metrics for "high-flow" estimation using hydrologic
747   models. *Hydrology and Earth System Sciences*, *23*(6). https://doi.org/10.5194/hess-23-2601-
748   2019

749 Musolff, A., Fleckenstein, J. H., Rao, P. S. C., & Jawitz, J. W. (2017). Emergent archetype
750   patterns of coupled hydrologic and biogeochemical responses in catchments. *Geophysical
751   Research Letters*, *44*(9). https://doi.org/10.1002/2017GL072630

752 Musolff, A., Schmidt, C., Selle, B., & Fleckenstein, J. H. (2015). Catchment controls on solute
753   export. *Advances in Water Resources*, *86*, 133–146.
754   https://doi.org/10.1016/j.advwatres.2015.09.026

755 Nash, J. E., & Sutcliffe, J. V. (1970). River flow forecasting through conceptual models part I -
756   A discussion of principles. *Journal of Hydrology*, *10*(3). https://doi.org/10.1016/0022-
757   1694(70)90255-6

758 Neitsch, S. ., Arnold, J. ., Kiniry, J. ., & Williams, J. . (2011). Soil & Water Assessment Tool
759   Theoretical Documentation Version 2009. *Texas Water Resources Institute*.
760   https://doi.org/10.1016/j.scitotenv.2015.11.063

761 Nguyen, T. V., Kumar, R., Lutz, S. R., Musolff, A., Yang, J., & Fleckenstein, J. H. (2021).
762   Modeling Nitrate Export From a Mesoscale Catchment Using StorAge Selection Functions.
763   *Water Resources Research*. https://doi.org/10.1029/2020wr028490

764 Nixdorf, E., & Trauth, N. (2018). Evaluating the reliability of time series analysis to estimate
765   variable riparian travel times by numerical groundwater modelling. *Hydrological Processes*,
766   *32*(3). https://doi.org/10.1002/hyp.11428

767 Pianosi, F., Beven, K., Freer, J., Hall, J. W., Rougier, J., Stephenson, D. B., & Wagener, T.
768   (2016). Sensitivity analysis of environmental models: A systematic review with practical
769   workflow. *Environmental Modelling and Software*, *79*, 214–232.
770   https://doi.org/10.1016/j.envsoft.2016.02.008

771 Pianosi, F., Sarrazin, F., & Wagener, T. (2015). A Matlab toolbox for Global Sensitivity
772   Analysis. *Environmental Modelling and Software*, *70*, 80–85.
773   https://doi.org/10.1016/j.envsoft.2015.04.009

774 Randall, G. W., & Mulla, D. J. (2001). Nitrate Nitrogen in Surface Waters as Influenced by
775   Climatic Conditions and Agricultural Practices. *Journal of Environmental Quality*.
776   https://doi.org/10.2134/jeq2001.302337x

777 Remondi, F., Kirchner, J. W., Burlando, P., & Fatichi, S. (2018). Water Flux Tracking With a
778   Distributed Hydrological Model to Quantify Controls on the Spatiotemporal Variability of
779   Transit Time Distributions. *Water Resources Research*, *54*(4), 3081–3099.
780   https://doi.org/10.1002/2017WR021689

781 Rinaldo, A., Benettin, P., Harman, C. J., Hrachowitz, M., McGuire, K. J., Van Der Velde, Y.,
782   Bertuzzo, E., & Botter, G. (2015). Storage selection functions: A coherent framework for
783   quantifying how catchments store and release water and solutes. In *Water Resources*
784   *Research*. https://doi.org/10.1002/2015WR017273

785 Samaniego, L., Kumar, R., & Attinger, S. (2010). Multiscale parameter regionalization of a grid-
786   based hydrologic model at the mesoscale. *Water Resources Research*, *46*(5), 1–25.
787   https://doi.org/10.1029/2008WR007327

788 Sarrazin, F., Hartmann, A., Pianosi, F., Rosolem, R., & Wagener, T. (2018). V2Karst V1.1: A
789   parsimonious large-scale integrated vegetation-recharge model to simulate the impact of
790   climate and land cover change in karst regions. *Geoscientific Model Development*, *11*(12).
791   https://doi.org/10.5194/gmd-11-4933-2018

792 Scanlon, T. M., Ingram, S. M., & Riscassi, A. L. (2010). Terrestrial and in-stream influences on
793   the spatial variability of nitrate in a forested headwater catchment. *Journal of Geophysical*
794   *Research: Biogeosciences*, *115*(G2). https://doi.org/10.1029/2009jg001091

795 Schaefli, B., & Gupta, H. V. (2007). Do Nash values have value? In *Hydrological Processes*
796   (Vol. 21, Issue 15). https://doi.org/10.1002/hyp.6825

797 Thorburn, P. J., Biggs, J. S., Weier, K. L., & Keating, B. A. (2003). Nitrate in groundwaters of
798   intensive agricultural areas in coastal Northeastern Australia. *Agriculture, Ecosystems and*
799   *Environment*. https://doi.org/10.1016/S0167-8809(02)00018-X

800 van der Velde, Y., Heidbüchel, I., Lyon, S. W., Nyberg, L., Rodhe, A., Bishop, K., & Troch, P.
801   A. (2015). Consequences of mixing assumptions for time-variable travel time distributions.
802   *Hydrological Processes*, *29*(16), 3460–3474. https://doi.org/10.1002/hyp.10372

803 van der Velde, Y., Torfs, P. J. J. F., Van Der Zee, S. E. A. T. M., & Uijlenhoet, R. (2012).
804   Quantifying catchment-scale mixing and its effect on time-varying travel time distributions.
805   *Water Resources Research*, *48*(6), 1–13. https://doi.org/10.1029/2011WR011310

806 Winter, C., Lutz, S. R., Musolff, A., Kumar, R., Weber, M., & Fleckenstein, J. H. (2021).
807   Disentangling the Impact of Catchment Heterogeneity on Nitrate Export Dynamics From

808   Event to Long-Term Time Scales. *Water Resources Research*.
809   https://doi.org/10.1029/2020WR027992

810   Wollschläger, U., Attinger, S., Borchardt, D., Brauns, M., Cuntz, M., Dietrich, P., Fleckenstein,
811   J. H., Friese, K., Friesen, J., Harpke, A., Hildebrandt, A., Jäckel, G., Kamjunke, N., Knöller,
812   K., Kögler, S., Kolditz, O., Krieg, R., Kumar, R., Lausch, A., … Zacharias, S. (2017). The
813   Bode hydrological observatory: a platform for integrated, interdisciplinary hydro-ecological
814   research within the TERENO Harz/Central German Lowland Observatory. *Environmental*
815   *Earth Sciences*, *76*(1). https://doi.org/10.1007/s12665-016-6327-5

816   Yang, J., Heidbüchel, I., Musolff, A., Reinstorf, F., & Fleckenstein, J. H. (2018). Exploring the
817   Dynamics of Transit Times and Subsurface Mixing in a Small Agricultural Catchment.
818   *Water Resources Research*, *54*(3), 2317–2335. https://doi.org/10.1002/2017WR021896

819   Yang, X., Jomaa, S., Zink, M., Fleckenstein, J. H., Borchardt, D., & Rode, M. (2018). A New
820   Fully Distributed Model of Nitrate Transport and Removal at Catchment Scale. *Water*
821   *Resources Research*, *54*(8), 5856–5877. https://doi.org/10.1029/2017WR022380

822   Zink, M., Kumar, R., Cuntz, M., & Samaniego, L. (2017). A high-resolution dataset of water
823   fluxes and states for Germany accounting for parametric uncertainty. *Hydrology and Earth*
824   *System Sciences*, *21*(3). https://doi.org/10.5194/hess-21-1769-2017

825